Histologic and Genomic Analysis of Conjunctival SCC in African and American Cohorts Reveal UV Light and HPV Signatures and High Tumor Mutation Burden

Frederico O. Gleber-Netto,[1] Priyadharsini Nagarajan,[2] Oded Sagiv,[1,5] Curtis R. Pickering,[1,†] Neil Gross,[1] Jing Ning,[4] Melisachew M. Yeshi,[6] Yonas Mitku,[7] Michael T. Tetzlaff,[2,‡] and Bita Esmaeli[3]

[1]Department of Head and Neck Surgery, The University of Texas MD Anderson Cancer Center, Houston, Texas, United States
[2]Department of Pathology, The University of Texas MD Anderson Cancer Center, Houston, Texas, United States
[3]Orbital Oncology and Ophthalmic Plastic Surgery, Department of Plastic Surgery, The University of Texas MD Anderson Cancer Center, Houston, Texas, United States
[4]Department of Biostatistics, The University of Texas MD Anderson Cancer Center, Houston, Texas, United States
[5]The Goldschleger Eye Institute, Sheba Medical Center, Tel Aviv University, Tel Aviv, Israel
[6]Department of Pathology, Mekelle University, Mekelle, Ethiopia
[7]Department of Ophthalmology, Mekelle University, Mekelle, Ethiopia

Correspondence: Bita Esmaeli, Orbital Oncology and Ophthalmic Plastic Surgery, Department of Plastic Surgery, The University of Texas MD Anderson Cancer Center, 1515 Holcombe Blvd, Unit 1488, Houston, TX 77030, USA; besmaeli@mdanderson.org.

FOGN, PN and OS contributed equally to this work.
Present affiliation: †Department of Surgery-Otolaryngology, Yale School of Medicine, New Haven, Connecticut, United States.
Present affiliation: ‡Department of Pathology, University of California - San Francisco, San Francisco, California, United States.

Received: October 12, 2023
Accepted: December 12, 2023
Published: April 10, 2024

Citation: Gleber-Netto FO, Nagarajan P, Sagiv O, et al. Histologic and genomic analysis of conjunctival SCC in African and American cohorts reveal UV light and HPV signatures and high tumor mutation burden. *Invest Ophthalmol Vis Sci.* 2024;65(4):24. https://doi.org/10.1167/iovs.65.4.24

Purpose. Conjunctival squamous cell carcinoma (conjSCC) is more prevalent and aggressive in sub-Saharan African countries compared with the rest of the world. This study aims to compare the genomic, immunophenotypic, and histologic features between patients from the United States and Ethiopia, to identify etiopathogenic mechanisms and unveil potential treatment strategies.

Methods. We compared histologic features and mutational profiles using whole exome sequencing, high-risk human papillomavirus (HPV) status, PD-L1 expression, and tumor-infiltrating lymphocytes in conjSCC tumors of patients from Ethiopia (ETH; $n = 25$) and the United States (from MD Anderson [the MDA cohort]; $n = 29$). Genomic alterations were compared with SCCs from other anatomic sites using data from The Cancer Genome Atlas.

Results. Solar elastosis was seen in 78% of ETH and 10% of MDA samples. Thicker tumors had higher density of CD8+ and CD3+ cells. HPV status was similar between the cohorts (ETH = 21% and MDA = 28%). The mean tumor mutation burden (TMB) was significantly higher in conjSCC (3.01/Mb, log10) and cutaneous SCC compared other SCC subtypes. ETH samples had higher TMB compared to the MDA cohort (3.34 vs. 2.73). Mutations in genes associated with ultraviolet light (UV) signature were most frequently encountered (SBS7b = 74% and SBS7a = 72%), with higher prevalence in the ETH cohort, whereas SBS2 and SBS13 signatures were more common among MDA HPV+ conjSCCs.

Conclusions. Our findings suggest that UV exposure may play a major role in conjSCC, with a higher prevalence in the ETH cohort compared with the MDA cohort, where HPV also contributes.

Keywords: conjunctival squamous cell carcinoma (conjSCC), genomic analysis, histopathologic analysis, tumor mutational burden (TMB), ultraviolet light (UV)

The epidemiology of conjunctival squamous cell carcinoma (conjSCC) varies by population and geographic location.[1,2] In Western/high-income countries, conjSCC is predominantly seen in elderly individuals in association with chronic ultraviolet (UV) radiation exposure, and a male preponderance. ConjSCC is also seen, albeit less frequently, in younger patients with chronic acquired immunosuppression, such as organ transplant recipients and patients with HIV infection.[3,4] In countries close to the equator, particularly the sub-Saharan Africa, most of which also happen to be low- and middle-income countries, the mean age at presentation of conjSCC is considerably lower with frequent female preponderance, and presents at a more advanced stage and is associated with worse outcomes.[5–11] Greater HIV prevalence and poorer access to health care have been postulated as possible explanations for these differences.[12,13] Human papilloma virus (HPV) infection is a risk factor for conjSCC,[12,14,15] with

high-risk HPV serotypes 16, 18, and 33 being the most commonly associated. A recent meta-analysis of 39 studies found an overall increased risk for conjunctival squamous carcinogenesis in patients with HPV infection (odds ratio [OR] = 8.4); however, the increased risk associated with HPV infection was much lower among patients from African countries (OR = 1.7).[16] Clinically, immunocompromised patients tend to have a more aggressive course with rapid tumor growth and a larger proportion of cases having ocular (globe) or orbital invasion and local recurrence.[1,4]

A few studies have explored the genomic and epigenetic drivers of conjSCC. In a recent study from India, UV-signature mutations were identified in the human telomerase reverse transcriptase (*TERT*) promoter in 6 of 19 patients (32%), and such mutations were associated with high American Joint Committee on Cancer (AJCC) T-category (>T3) and shorter disease-free survival.[17] In an East Asian cohort of 31 patients, transcriptomic comparison between carcinoma in situ and advanced disease revealed significant differences in the expression of 45 genes, with thrombospondin-1 (*THBS1*) being the most biologically important.[18] In a study of 41 Ugandan patients, *TP53* codon 72 polymorphisms were found to be an independent risk factor for high-grade conjunctival intraepithelial neoplasia and invasive conjSCC, regardless of HIV status.[19] In a report from Saudi Arabia, *TP53* overexpression was found in 14 of 23 (61%) conjSCCs and correlated with poor clinical outcome.[20] Another study compared 11 conjSCC specimens from Saudi Arabia to 3 normal conjunctival specimens from the United States and revealed upregulation of *MMP9*, *MMP11*, and *S100A2* and downregulation of clusterin (*CLU*) in the conjSCC.[21] Almost all of these studies were limited to one population and/or geographic region. We hypothesized that systematic genomic comparison of Western and African patient cohorts could reveal biologically significant differences and explain the distinct prognosis in patients with conjSCC in sub-Saharan Africa.

Immune checkpoint inhibitors are a relatively new therapeutic strategy for patients with cutaneous squamous carcinoma.[22–24] A recent multi-institutional trial revealed that neoadjuvant treatment with up to 4 doses of cemiplimab (PD1 inhibitor) resulted in a complete pathologic response in 51% of patients, in addition to a major pathological response in 13% of patients.[22] Similarly, inhibition of the PD1/PD-L1 axis has shown promise in the neoadjuvant and adjuvant management of periocular SCC.[25] These results have raised the possibility of using immune checkpoint blockade for the management of conjSCC. In our previous study, we noted immunohistochemical expression of PD-L1 in 47% of specimens of conjSCC,[26] which correlated with higher AJCC T-category and higher density of T-lymphocytes expressing CD3, CD8, and PD1, but not with high-risk HPV status.[26]

In the current study, to determine whether there are differences in etiology between conjSCC in sub-Saharan African and Western countries and to try to identify potential new targets for treating conjSCC, we compared histologic features, mutational profile with respect to tumor mutation burden (TMB) and genomic signatures, high-risk HPV status, PD-L1 expression, and density and composition of tumor-infiltrating lymphocytes (TILs) in conjSCC tumors from two cohorts of patients, one from Ethiopia and the other from the United States.

Methods

Cohort and Tissue Samples

The study was approved by the Institutional Review Boards of The University of Texas MD Anderson Cancer Center, Houston, TX, USA, and Mekelle University, Mekelle, Ethiopia, and performed in accordance with the Declaration of Helsinki. Some patients and samples from our previous study focused on PD-L1 expression were included in the current study.[26] Only patients with adequate amounts of remnant archival formalin-fixed, paraffin-embedded (FFPE) tissue (beyond that required for routine patient care) were included. The study included 29 patients from MD Anderson, hereafter referred to as the MDA cohort (diagnosed in 2009–2019), and 25 from Mekelle University, hereafter referred to as the ETH cohort. Control tissues, such as negative lymph nodes or adjacent uninvolved conjunctiva, were also collected for the MDA cohort, when available ($n = 13$); control tissues were not available for ETH cohort samples. Demographic, clinical, histopathologic, and follow-up data were collected; however, the demographic and clinical information for the ETH cohort were not accessible at the time of this study because of a major conflict and war in Ethiopia. In the MDA cohort, three cases had only metastatic samples available for sequencing; for these cases, histopathologic features, including solar elastosis, of the respective primary tumors were collected from patient records. For the ETH cohort, the histopathologic characteristics were documented based on a single representative tumor block, identified as having the greatest tumor volume based on examination of all tumor sections (by authors P.N. and M.M.Y.).

Immunohistochemistry, In Situ Hybridization, and Image Analysis

Immunohistochemical studies were performed on 4-µm-thick tissue sections using a Leica Bond III autostainer, using the following antibodies: CD3 (Dako A0452; 1:100 dilution), CD8 (Life Sciences Technology MS457s; 1:25 dilution), PD1 (Abcam ab137132; 1:250 dilution), and PD-L1 (Cell Signaling Technology 13684S; 1:100 dilution). RNA in situ hybridization to identify high-risk HPV types (16, 18, 31, 33, 35, 45, 52, and 58) was performed using the RNAscope 2.5 LS assay. One ETH sample could not be tested for PD-L1 and high-risk HPV status due to exhaustion of tumor.

PD-L1 expression was determined by microscopic evaluation and determination of tumor proportion score (TPS), defined as the percentage of tumor cells that displayed complete or partial membranous staining, and tumors with at least 1% of tumor cells positive were considered PD-L1 positive. High-risk HPV status was determined by identification of punctate signals at 100 × magnification.[26] Automated image analysis for quantification of lymphocytes expressing CD3, CD8, and PD1 was performed as described previously.[26] Briefly, 3 to 5 0.25-mm^2 regions of interest (ROIs) encompassing tumor-stroma interface with progressively decreasing density of immune infiltrate were identified on each immunohistochemical slide scanned at 200 × magnification using the Aperio Scanscope AT Turbo (Leica Biosystems). To ensure optimal image analysis of tumor-associated immune infiltrate, the ROIs were first selected on a CD3-immunohistochemical slide and then the corresponding ROIs were designated on CD8 and PD1 slides for each sample. Positive cells were enumerated using the

Investigative Ophthalmology & Visual Science

Aperio ImageScope image analysis software (Leica Biosystems), and density was reported as the average number of cells per mm^2 for each sample.

Whole Exome Library Preparation and Sequencing

Samples from both institutions were processed and analyzed at MD Anderson. For each sample, representative areas of tumor (ETH, $n = 25$ and MDA, $n = 29$) and, when available, normal tissue (MDA, $n = 13$) were selected and circled on a hematoxylin and eosin–stained slide. These were used as a guide for manual microdissection performed on 10 to 20 unstained 5-mm FFPE sections. The genomic DNA was extracted using the PicoPure DNA Extraction Kit (Arcturus) and purified using the AMPureXP Kit (Agencourt Biosciences). For samples for which corresponding normal tissue was not available, a pool of peripheral blood DNA from 11 healthy individuals was used as a normal reference.

Whole exome libraries were created from the extracted DNA using the hybridization capture–based target enrichment sequencing panel SureSelect Human All Exon V4 (Agilent Technologies, Inc.), which targets 51 Mb of the human genome (human genome assembly GRCh37/hg19) covering exonic regions from 20,965 genes, and then sequenced on a HiSeq4000 sequencer (Illumina Inc.).

Whole Exome Sequencing Data Processing

Raw sequencing files (BLC files) were processed using Illumina's Consensus Assessment of Sequence and Variation (CASAVA) tool and converted to FASTQ files. These were aligned to the reference genome (GRCh37/hg19) using BWA[27] and pre-processed using GATK.[28] Somatic mutation calling was performed with the MuTect algorithm.[29] To exclude germline events, we used whole exome data generated from either paired normal tissue or the above-mentioned DNA pool from 11 healthy individuals (with 200 × coverage) as a reference.

The following were excluded: variants with coverage less than 20 × for tumor samples and less than 10 × for normal samples, variants with allele fraction less than 0.02, variants reported in the EXAC,[30] 1000 Genomes Project,[31] or gnomAD[32] database with allele fraction greater than 0.01 in any population, and potential technical artifacts (e.g. low allele frequency and low coverage) were visually identified using the IGV tool.[33] Although single nucleotide variants can be reliably detected from FFPE-derived DNA samples, identification of insertions and deletions (INDELs) and long variants from this type of sample are less accurate.[34,35] Because all our samples were taken from FFPE tissue and we did not have matched normal controls for the samples in the ETH cohort, we decided to also exclude INDELs and oligonucleotide polymorphisms from our analysis.

Whole Exome Sequencing Data Analyses

Filtered conjSCC variants were organized and analyzed in the R environment for statistical computing with the package Maftools (version 2.16.0)[36] and its dependencies, which assisted with data visualization, estimation of the TMB, and assessment of APOBEC-related mutation signature enrichment.[37]

Additionally, the SigProfilerBioinformatic Tools (https://cancer.sanger.ac.uk/signatures/tools/; accessed July 2022) from the Catalogue of Somatic Mutations in Cancer (COSMIC) were used to identify the mutation signature profiles and patterns of mutation clustering in conjSCC.

Initially, matrices of somatic mutations were created with the SigProfilerMatrixGenerator,[38] which takes into account the 6 possible single base substitutions (SBSs: C>T, C>G, C>T, T>A, T>C, and T>G), using the pyrimidine base as reference, as well as the immediate 5′ and 3′ bases flanking each substitution, resulting in matrices of 96 unique mutation patterns. Next, de novo mutation signatures were extracted from these matrices using the SigProfilerExtractor tool using Python.[39] This tool uses non-negative matrix factorization to decode the number of distinct de novo mutation signatures in the cohort and the relative frequency of each pattern in the individual samples. Finally, the de novo mutation signatures were decomposed into the COSMIC SBS signatures.

Additionally, the SigProfilerClusters tool was used to identify clustered mutations according to the intermutational distances (IMDs) across each sample genome. A sample-dependent IMD threshold is calculated considering each sample TMB and mutation patterns, leading to the categorization of mutations from a given patient into clustered mutations (above the sample-specific IMD threshold) and non-clustered mutations (below the sample-specific IMD threshold). Then, clustered events are subclassified into two groups based on the number of and distance between clustered events. For our study, adjacent mutations (IMD = 1) and clusters with 3 or fewer mutations were classified as small clustered events and comprised doublet base substitutions, multi-base substitutions, and omikli events, which are represented by 2 or 3 mutations distributed with an IMD greater than 1 and below the sample-dependent IMD threshold. Diffuse hypermutation events formed by clusters of four or more mutations, named kataegis, were classified as larger clustered events.[40]

In Silico Comparison of ConjSCC With Other SCC Subtypes

We compared the conjSCC genomic alterations with those of SCCs from other organs using data from The Cancer Genome Atlas (TCGA). Because these studies included several histologic variants, we selected only SCC samples, as described by Campbell et al.[41] We used the R package TCGA mutations[42] to retrieve whole exome sequencing data from TCGA studies, including studies of urinary bladder ($n = 47$),[43] uterine cervix ($n = 241$),[43] esophagus ($n = 95$),[43] head and neck ($n = 501$),[43] lungs ($n = 471$),[43] and skin ($n = 83$).[42,44] The list of included samples is described in Supplementary Table S1. Next, we extracted the mutation frequency information from conjSCC and TCGA samples focusing on a curated list of cancer driver genes described by Bailey et al.[45] The distribution of mutations in these genes and their respective pathways was compared among the studied cohorts.

Results

Histopathologic and immunophenotypic characteristics of the cases included in the study (ETH, $n = 25$ and MDA, $n = 29$) are summarized in Table 1 and Figure 1. All the ETH samples were from primary tumors, including 6 in situ

Table 1. Histopathologic Characteristics of the ETH and MDA Cohorts*

Variable	ETH (n = 25) n (%)	MDA (n = 29) n (%)	Pearson P Value
Tumor type			0.219
In situ	6 (24)	8 (28)	
Invasive	19 (76)	18 (62)	
Metastatic	0 (0)	3 (10)	
Highest histologic grade			0.520
G1 (well differentiated)	1 (4)	4 (14)	
G2 (moderately differentiated)	17 (68)	15 (52)	
G3 (poorly differentiated)	6 (24)	8 (28)	
G4 (spindled/sarcomatoid)	1 (4)	2 (7)	
Maximum tumor size, cm†			0.283‡
<2	12 (67)	6 (43)	
≥2	6 (33)	8 (57)	
Tumor thickness, mm†			0.043‡
<5	15 (83)	10 (48)	
≥5	3 (17)	11 (52)	
PNI†			0.021‡
Not identified	19 (100)	15 (71)	
Present	0 (0)	6 (29)	
LVI†			1.00‡
Not identified	19 (100)	20 (95)	
Present	0 (0)	1 (5)	
Solar elastosis grade§			<0.001
None	4 (22)	26 (90)	
Mild	2 (11)	0 (0)	
Moderate	3 (17)	1 (3)	
Severe	9 (50)	2 (7)	
High-risk HPV status			0.750‡
Negative	19 (79)	21 (72)	
Positive	5 (21)	8 (28)	
PD-L1 expression in tumor			0.394‡
Negative (<1%)	11 (46)	9 (31)	
Positive (≥1%)	13 (54)	20 (69)	

LVI, lymphovascular invasion; PNI, perineural invasion.

* Values in table are number of patients (percentage). As noted in Figure 1A, not all histopathologic characteristics were available for all patients.

† Not calculated for conjSCC in situ tumors.

‡ The P value was calculated by the Fisher's exact test.

§ Solar elastosis could not be assessed since the tissue available for evaluation is composed entirely of tumor in the representative block.

and 19 invasive carcinomas, whereas the MDA samples were from 26 primary tumors (8 in situ and 18 invasive) and 3 metastatic tumors.

Histopathologic Characteristics

The majority of the conjSCCs were moderately differentiated, and the ETH and MDA cohorts had similar rates of HPV positivity (21% and 28%, respectively, P = 0.750; see Table 1, Fig. 1A). HPV status did not correlate with primary tumor histopathologic features (Supplementary Table S2). Perineural invasion (PNI) was not detected in the ETH cohort but was present in 29% of the primary invasive conjSCCs in the MDA cohort (P = 0.021). The proportion of tumors positive for PD-L1 expression did not differ significantly between the two cohorts (ETH = 54% and MDA = 69%).

Conjunctival subepithelial/stromal solar elastosis was present in a higher proportion of ETH samples (n = 14, 78%) than MDA samples (n = 3, 10%, P < 0.001, Fisher's exact test; see Table 1, Figs. 1B–D). We further grouped the cases with solar elastosis according to grade based on the relative stromal area and the proportion of stromal collagen fibers involved by solar elastosis (Supplementary Fig. S1). In both cohorts, when solar elastosis was present, it was most often severe (see Table 1, Fig. 1C). We then compared solar elastosis with HPV status (Table 2, Fig. 1D). Among the HPV-negative (HPV–) tumors, the rate of solar elastosis was significantly higher among the ETH samples (77%, n = 10) than among the MDA samples (14%, n = 3, P = 0.0006). Among the HPV-positive (HPV+) tumors, the rate of solar elastosis was also significantly higher among the ETH samples (75%, n = 3) than among the MDA samples (0%, P = 0.018), with all cases classified as severe. No major pathological differences were observed between HPV+ and HPV– tumors within the ETH cohort or the MDA cohort.

Tumor-Infiltrating T-Lymphocytes

The density of TILs did not differ significantly between the two cohorts or by primary tumor size (Table 3, Fig. 1E). However, thicker tumors had significantly higher density of CD8+ and CD3+ cells and a trend toward higher density of PD1+ cells (P = 0.0005, P = 0.002, and P = 0.051, respectively). The density of CD3+ cells was significantly higher in tumors with PNI than in those without (Wilcoxon P = 0.018); there was no correlation between CD3+ cell density and with lymphovascular invasion (LVI). Tumors arising in a background of conjunctival solar elastosis had significantly

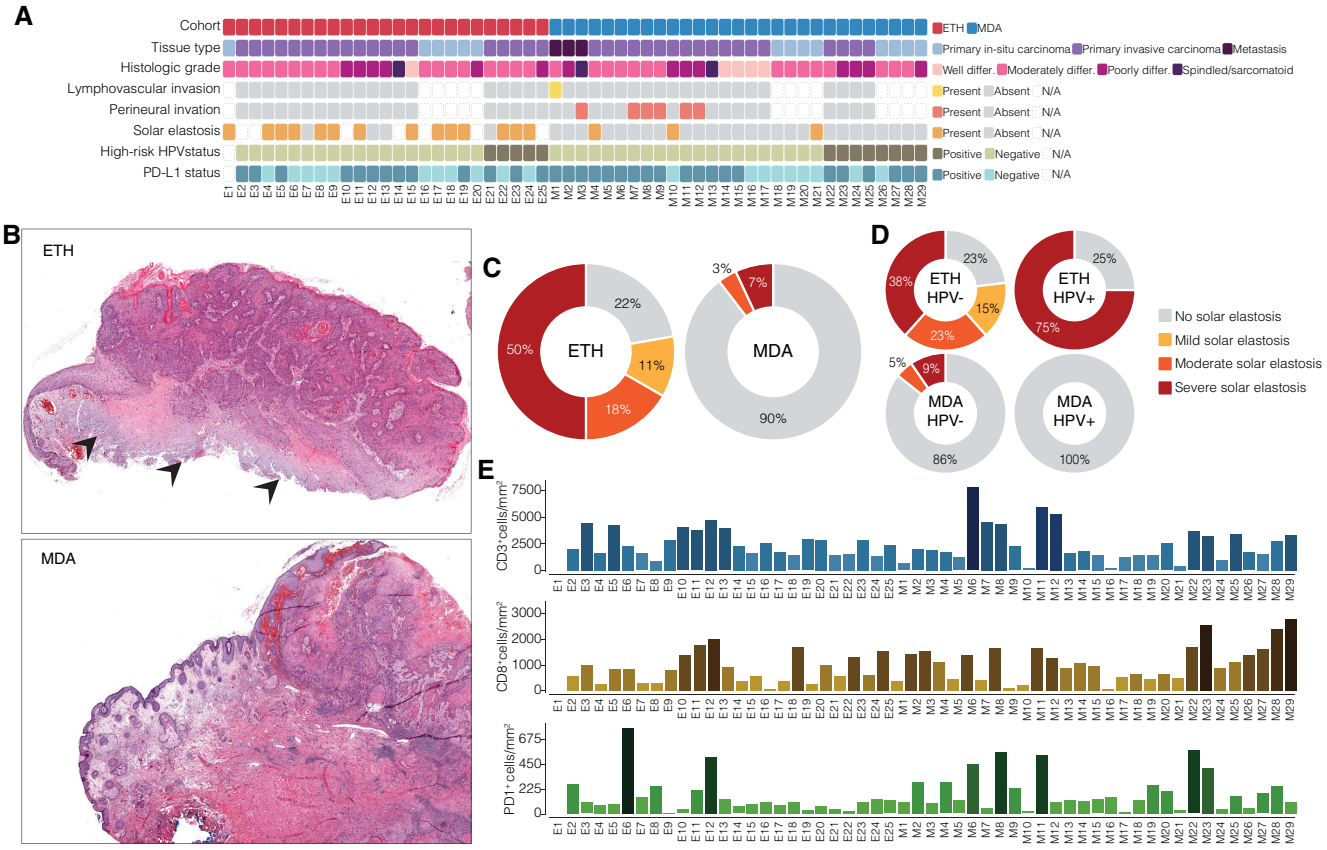

Figure 1. Histopathologic characteristics of samples in the ETH and MDA cohorts. (**A**) Cohort and histologic characteristics, showing country of origin (ETH, MDA), type of conjSCC (primary: in situ/invasive/ metastatic), histologic grade, presence of lymphovascular invasion (LVI), perineural invasion (PNI), conjunctival subepithelial/ stromal solar elastosis, high-risk human papilloma virus (HPV) status, and PD-L1 (tumor proportion score ≥1%). (**B**) Histologic images of representative conjSCCs with severe conjunctival subepithelial/stromal solar elastosis (*arrowheads*, *top panel*, magnification 10 × in the ETH cohort) and without solar elastosis (*bottom panel*, magnification 10 ×, in the MDA cohort). (**C, D**) Prevalence and severity of solar elastosis in the ETH and MDA cohorts (**C**) and by HPV status (**D**). (**E**) Density of tumor-infiltrating lymphocytes (average number of cells/mm^2) expressing CD3 (*top panel*), CD8 (*middle panel*), and PD1 (*bottom panel*). Each column corresponds to the sample in the corresponding column of panel **A**.

lower density of CD8+ and PD1+ cells ($P = 0.026$ and $P = 0.041$, respectively). Whereas CD3+ cell density was also lower among samples with solar elastosis, this difference was not statistically significant.

Analysis of tumors from the ETH and MDA cohorts together showed that HPV+ conjSCCs had a significantly higher density of CD8+ cells ($P = 0.0028$). We then grouped samples according to cohort and HPV status, which revealed significant differences in CD8+ cell density ($P = 0.009$; see Supplementary Table S2). Within the MDA cohort, CD8+ cell density was higher in HPV+ samples than in HPV– samples ($P = 0.024$). CD8+ cell density was much higher among MDA HPV+ tumors than among ETH HPV– tumors ($P = 0.006$). Interestingly, within the ETH cohort, no significant association was observed between HPV status and CD8+ cell density (Supplementary Table S3).

PD-L1-positive tumors exhibited significantly higher density of CD3+, CD8+, and PD1+ cells than PD-L1-negative tumors did (Wilcoxon $P = 0.0001$, $P < 0.0001$, and $P = 0.044$, respectively; see Table 3, Supplementary Table S4). Similar trends were observed when each cohort was evaluated independently, except that PD1+ cell density did not differ between PD-L1-positive and PD-L1-negative tumors in the ETH cohort.

Number and Types of Mutations

The mean (SD) total number of mutations was higher in the ETH cohort (4335.7 [2090.4], range = 131 to 14,579) than in the MDA cohort (1997.3 [3005.4], range = 1210 to 9557, $P < 0.0001$; Fig. 2A). The mutated genes in each group are listed in Supplementary Table S5. Overall, 15,078 distinct genes were mutated among the ETH samples, and 12,010 distinct genes were mutated among the MDA samples. Of 16,655 genes mutated in one or both cohorts, 10,433 (62.6%) were mutated in both cohorts, 4645 (27.9%) were mutated in the ETH cohort only, and 1577 (9.5%) were mutated in the MDA cohort only. Some of the most frequently mutated genes in the conjSCC samples from both cohorts are also commonly mutated in other cancers (see the flagged genes in Supplementary Table S5). Although their connection to cancer is not yet clear, many of these genes have been linked to various human illnesses. As their significance in conjSCC biology cannot be ruled out, they were included in the subsequent analyses.

Considering only the 2128 genes mutated in at least 25% of tumors in each cohort, the proportion of genes mutated uniquely among ETH samples was very high; specifically, 169 genes (7.9%) were mutated in both

Table 2. Correlation Between High-Risk HPV Status and Histologic Characteristics of the Cohorts[*]

Variable	ETH HPV− *n* (%)	MDA HPV− *n* (%)	ETH HPV+ *n* (%)	MDA HPV+ *n* (%)	ETH Versus MDA HPV− *n* (%)	ETH Versus MDA HPV+ *n* (%)	HPV+ Versus HPV− ETH *n* (%)	HPV+ Versus HPV− MDA *n* (%)
Tumor type					0.221	0.105[†]	0.544[†]	0.181
In situ	5 (26)	4 (19)	0 (0)	4 (50)				
Invasive	14 (74)	14 (67)	5 (100)	4 (50)				
Metastatic	0 (0)	3 (14)	0 (0)	0 (0)				
Highest histologic grade					0.533	0.565[†]	0.859	0.230
G1 (well differentiated)	1 (5)	4 (19)	0 (0)	0 (0)				
G2 (moderately differentiated)	12 (63)	11 (52)	4 (80)	4 (50)				
G3 (poorly differentiated)	5 (26)	4 (19)	1 (20)	4 (50)				
G4 (spindled/sarcomatoid)	1 (5)	2 (10)	0 (0)	0 (0)				
Maximum tumor size, cm					0.214[†]	1.00[†]	0.615[†]	0.245[†]
<2	8 (62)	3 (30)	4 (80)	3 (75)				
≥2	5 (38)	7 (70)	1 (20)	1 (25)				
Tumor thickness, mm					0.229[†]	0.048[†]	1.00[†]	0.090[†]
<5	11 (85)	10 (59)	4 (80)	0 (0)				
≥5	2 (15)	7 (41)	1 (20)	4 (100)				
PNI					**0.021**[†]	—	—	0.281[†]
Not identified	14 (100)	11 (65)	5 (100)	4 (100)				
Present	0 (0)	6 (35)	0 (0)	0 (0)				
LVI					1.00[†]	—	—	1.00[†]
Not identified	14 (100)	16 (94)	5 (100)	4 (100)				
Present	0 (0)	1 (6)	0 (0)	0 (0)				
Solar elastosis					**<0.001**[†]	**0.018**[†]	1.00[†]	0.540[†]
Absent	3 (23)	18 (86)	1 (25)	8 (100)				
Present	10 (77)	3 (14)	3 (75)	0 (0)				
Solar elastosis grade					**0.003**	**0.018**[†]	0.492	0.529
None	3 (23)	18 (86)	1 (25)	8 (100)				
Mild	2 (15)	0 (0)	0 (0)	0 (0)				
Moderate	3 (23)	1 (5)	0 (0)	0 (0)				
Severe	5 (38)	2 (10)	3 (75)	0 (0)				

LVI, lymphovascular invasion; PNI, perineural invasion.
[*] One ETH sample could not be tested for high-risk HPV status due to exhaustion of tumor.
[†] The *P* value was calculated by the Fisher's exact test.

cohorts, 1950 (91.6%) were mutated in the ETH cohort only, and 9 (0.4%) were mutated in the MDA cohort only.

To contextualize the conjSCC mutations in terms of oncogenic potential, we compared our gene list against the catalog of driver genes (released on February 1, 2020) from the intOGen database (https://www.intogen.org/).[46] The top 20 mutant genes with potential oncogenic roles are shown in the mutation plot in Figure 2B, and the mutation frequency for the remaining predicted oncogenes in conjSCC samples is described in Supplementary Table S5. We found that of the 568 oncogenes described in the intOGen catalog, 521 (91.7%) were mutated in our conjSCC samples, including 480 (84.5%) mutated in the ETH tumors and 427 (75.2%) mutated in the MDA tumors. Most of these oncogenes (420/568) had a higher mutation rate among the ETH tumors than among the MDA tumors. This tendency can be seen in the mutation plot in Figure 2C, in which a higher proportion of ETH samples than MDA samples have mutations in the depicted oncogenes.

Association of Mutations With HPV Status

Next, we evaluated the role of HPV infection in the landscape of genomic alterations in conjSCC (see Fig. 2). The mean (SD) number of mutations tended to be higher in HPV– conjSCCs (2025.9 [1901.3]) than in HPV+ conjSCCs (1538.5 [1819.8], $P = 0.203$). However, the difference between HPV– and HPV+ tumors was primarily driven by the MDA samples. In the ETH cohort, the mean (SD) number of mutations was similar in HPV– tumors (2961.8 [2141.2]) and HPV+ tumors (2758.0 [2007.6], $P = 0.831$). On the other hand, in the MDA cohort, the mean (SD) number of mutations was higher in HPV– tumors (1179.1 [1156.5]) than in HPV+ tumors (776.4 [1283.7], $P = 0.137$). Importantly, the mutation rate was higher among ETH samples than among MDA samples, irrespective of HPV status. The mutation rate was higher among ETH HPV– tumors than among MDA HPV– tumors ($P < 0.001$) and was higher among ETH HPV+ tumors than among MDA HPV+ tumors ($P = 0.164$).

With respect to the mutation frequency of individual genes, our analyses revealed 60 genes differentially mutated between HPV+ and HPV– cases (with uncorrected $P < 0.05$; Supplementary Table S6). Mutations in *PIK3CA* are frequently found in HPV+ head and neck cancers, and were found in four HPV+ conjSCCs but no HPV– cases in our cohort.

In the MDA cohort, *TP53* mutations were more common among HPV– samples (71.4%, $n = 15$) than among MDA HPV+ samples (25%, $n = 2$). In the ETH cohort,

Table 3. Correlation Between Histopathologic Characteristics and Tumor-Infiltrating Lymphocytes

Variable	*n*	CD3+ Cell Density Cells/mm² Mean (SD)	*P* Value*	CD8+ Cell Density Cells/mm² Mean (SD)	*P* Value*	PD1+ Cell Density Cells/mm² Mean (SD)	*P* Value*
Cohort			0.3391		0.1453		0.1059
ETH	24	2541 (1117)		806 (562)		147 (171)	
MDA	29	2412 (1789)		1091 (714)		197 (164)	
Maximum tumor size, cm			0.279		0.3927		0.8345
<2	18	2556 (1326)		960 (604)		195 (199)	
≥2	14	3089 (1449)		1091 (614)		210 (195)	
Tumor thickness, mm			**0.0024**		**0.0005**		0.0515
<5	25	1978 (1189)		702 (480)		151 (170)	
≥5	14	3792 (1818)		1393 (529)		260 (201)	
PNI			**0.0179**		0.4154		0.5074
Present	6	4024 (1616)		1103 (682)		262 (228)	
Absent	34	2365 (1554)		912 (580)		180 (177)	
LVI			0.1408		0.3406		0.6649
Present	1	623 (NA)		367 (NA)		104 (NA)	
Absent	39	2665 (1644)		956 (591)		194 (187)	
Solar elastosis			0.2835		**0.026**		**0.0412**
Present	16	1945 (1127)		702 (473)		142 (188)	
Absent	30	2644 (1737)		1162 (717)		207 (167)	
High-risk HPV status			0.8605		**0.0028**		0.9753
Negative	40	2526 (1661)		790 (548)		177 (171)	
Positive	13	2301 (931)		1490 (715)		168 (161)	
PD-L1 expression			**0.0001**		**<0.0001**		**0.0445**
Negative (<1%)	20	1523 (793)		511 (316)		131 (169)	
Positive (≥1%)	33	3045 (1559)		1235 (666)		201 (163)	

LVI, lymphovascular invasion; PNI, perineural invasion.
* The *P* values were based on the Wilcoxon rank-sum test; those that are statistically significant are in the bolded font; and those approaching statistical significance are underlined.

the frequency of *TP53* mutations was similar among HPV+ samples (80%, $n = 4$) and HPV– samples (94.7%, $n = 18$).

Interestingly, none of the genes differentially mutated between MDA HPV+ and MDA HPV– tumors were differentially mutated between ETH HPV+ and ETH HPV– tumors, and vice versa (see Supplementary Table S6). For instance, genes commonly mutated among HPV– squamous tumors, such as *FAT1* (80%), *FAT3* (80%), and *CDKN2A* (60%),[47] had high mutation rates among ETH HPV+ cases but were not mutated among MDA HPV+ cases. Moreover, transitions were more common in ETH samples, irrespective of HPV status. Transversions were most common in MDA HPV+ samples compared to HPV– conjSCC.

Mutation Signature Analyses

Analyses of the overall mutational profiles of the 54 conjSCC samples revealed 3 distinct mutation patterns, which were decomposed into 7 COSMIC SBS signatures: SBS1 (proposed etiology: spontaneous deamination of 5-methylcytosine/clock-like signature) detected in 53 cases (98%), SBS5 (unknown etiology/clock-like signature) detected in 49 cases (91%), SBS7b (proposed etiology: UV light exposure) detected in 40 cases (74%), SBS7a (proposed etiology: UV light exposure) detected in 39 cases (72%), SBS13 (proposed etiology: activity of APOBEC family of cytidine deaminases) detected in 8 cases (15%), SBS10b (proposed etiology: polymerase epsilon exonuclease domain mutations) detected in 7 cases (13%), and SBS2 (proposed etiology: activity of APOBEC family of cytidine deaminases) detected in 6 cases (11.1%; see Figs. 2C, 2D, Supplementary Fig. S2).

In terms of the absolute number of mutations categorized in each SBS signature, SBS7b events were responsible for the largest fraction of the TMB for conjSCCs (mean [SD] mutations per tumor, 1052.5 [113.7]), followed by SBS7a (326.2 [399.8]) and SBS5 (184.4 [133.9]). With respect to the relative frequency of mutations from each SBS signature per tumor, the SBS7b signature was the most prevalent in 37 tumors (69%), followed by SBS5 ($n = 10$, 19%), SBS13 ($n = 3$, 6%), SBS1 ($n = 1$, 2%), SBS7a ($n = 1$, 2%), SBS10b ($n = 1$, 2%), and combination of SBS13 and SBS2 ($n = 1$, 2%; Fig. 2D). With respect to the relative frequency of each mutation signature per sample, SBS7b was the most frequent signature in the majority of ETH ($n = 22$, 88%) and MDA ($n = 15$, 55%) samples, followed by SBS5 (ETH: $n = 3$, 12% and MDA: $n = 7$, 24%).

We found significant differences in the frequency of mutation signatures between the ETH and MDA cohorts. SBS7b (ETH = 43,310, had 64.6% of all mutations and MDA = 13,529, had 46.9% of all mutations) and SBS7a (ETH = 11,402, had 17% of all mutations and MDA = 6212, had 21.5% of all mutations) represented the highest fraction of mutations in both cohorts. However, mutations with the SBS2, SBS10b, and SBS13 signatures that represented 7.8% ($n = 2250$) of all MDA mutations were notably absent in the ETH cohort.

We then compared the SBS signatures of the ETH and MDA cohorts according to their HPV status (see Fig. 2D, Supplementary Table S6). In the ETH cohort, SBS7b was the most prevalent mutation signature, irrespective of HPV status. However, in the MDA cohort, we observed signifi-

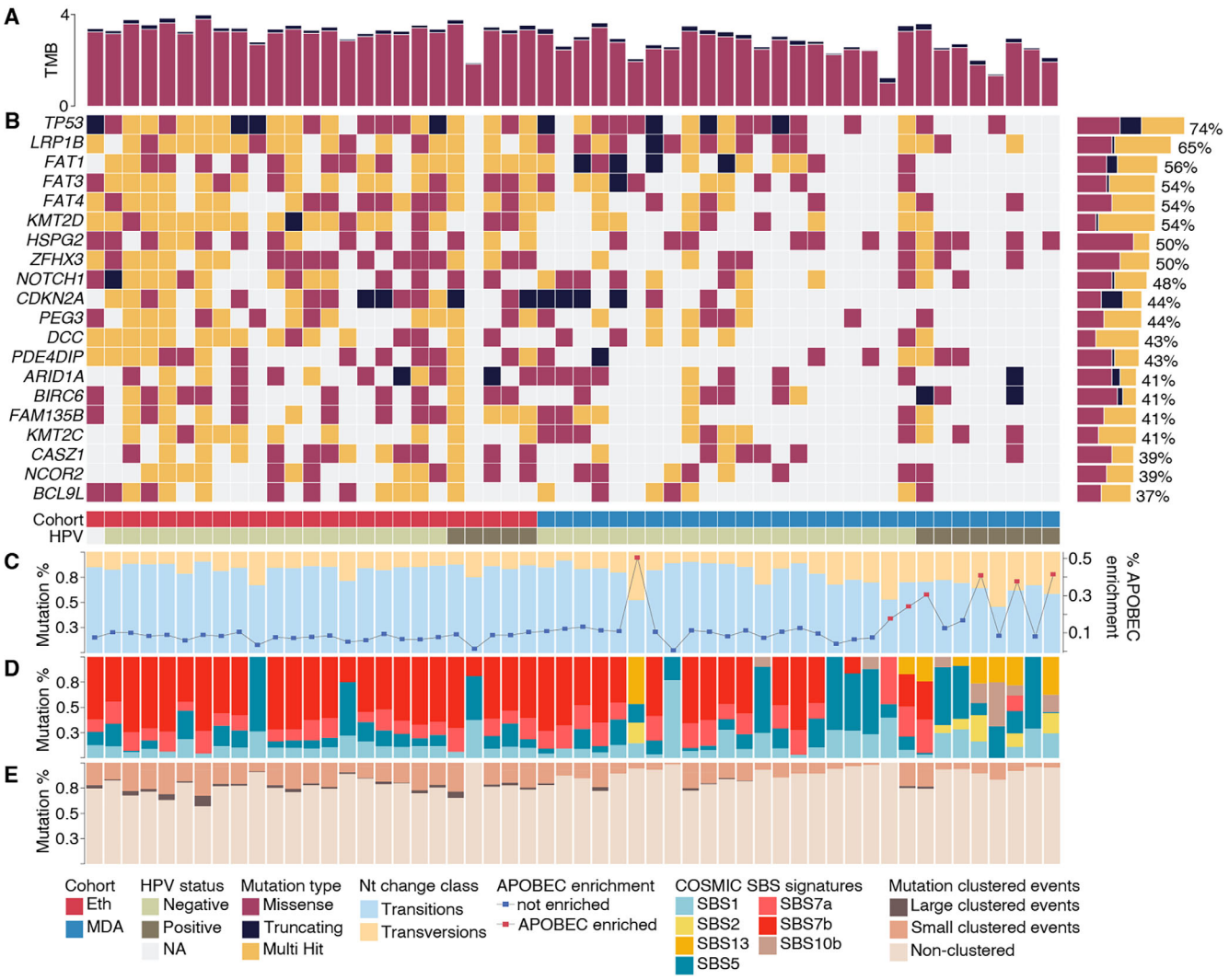

Figure 2. Mutation profile of conjSCC samples in the ETH and MDA cohorts with respect to high-risk HPV status. (**A**) TMB (number of mutations per sequenced mega base, log 10). (**B**) Mutations and mutation types in the 20 most mutated genes. The bar plot to the right shows the frequency of conjSCC samples with mutations in each gene displayed. (**C**) Frequency of nucleotide change class (transitions and transversions) (*bars*) and frequency of APOBEC-related mutation signature enrichment (*line*) per sample. (**D**) Frequency of mutations according to their COSMIC SBS signature class. (**E**) Frequency of clustered and non-clustered mutations per sample.

cant differences in the distribution of mutation signatures between HPV+ and HPV– cases. Whereas SBS2 ($P = 0.001$), SBS10b ($P = 0.002$), and SBS13 signatures were more prevalent in HPV+ cases, SBS7b ($P = 0.005$) and SBS7a ($P = 0.057$) signatures were more prevalent in HPV– cases.

We next compared the SBS signatures of the ETH and MDA cohorts according to their solar elastosis status (Supplementary Table S7). In the ETH cohort, the frequency of mutations with the SBS1 and SBS5 signatures was significantly higher in tumors with solar elastosis ($P = 0.022$ and $P = 0.022$, respectively), whereas the frequency of mutations with the SBS7a and SBS7b signatures tended to be lower in tumors with solar elastosis ($P = 0.099$ and $P = 0.079$, respectively). On the other hand, in the MDA cohort, the frequency of SBS7a mutations was significantly higher in tumors with solar elastosis ($P = 0.028$).

ETH samples had significantly higher frequencies of small and larger clustered events compared to MDA samples ($P < 0.001$ and $P < 0.001$, respectively; Fig. 2E). Within each cohort, the frequency of clustered events did not differ by HPV status. However, in the MDA cohort, small and larger clustered events were significantly more frequent in samples with solar elastosis than in those without solar elastosis ($P = 0.016$ and $P = 0.003$, respectively; see Supplementary Table S7). No significant differences were observed between MDA samples with elastosis and ETH samples with or without elastosis.

Association of Mutations With TILs

In the ETH cohort, the density of CD8+ T cells was positively correlated with the number of SBS7b mutations per sample (Spearman rho = 0.40, $P = 0.049$) but negatively correlated with the rate of SBS5 mutations per sample (Spearman rho = −0.48, $P = 0.015$). In the MDA cohort, the density of CD8+ T cells was positively correlated with the number of SBS2 mutations per sample (Spearman rho = 0.37, $P = 0.046$; Supplementary Table S8), which may

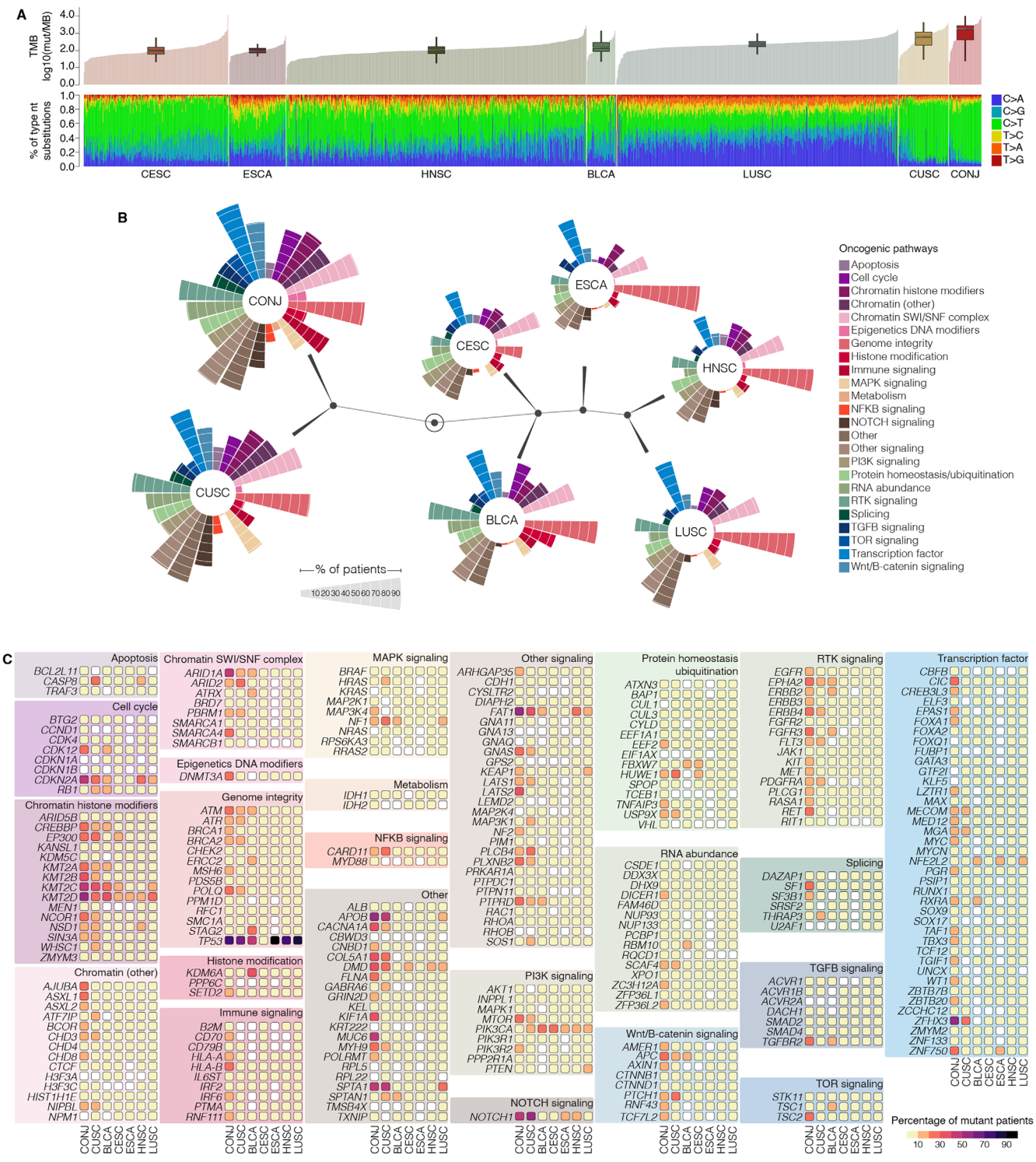

Figure 3. Comparison of genomic profiles of conjSCCs and SCCs arising in other organs. (**A**) *Top panel*: TMB for SCCs arising in various sites (number of mutations per sequenced mega base [Mb], log 10). CESC, uterine cervix; ESCA, esophagus; HNSC, head and neck; BLCA, urinary bladder; LUSC, lung; CUSC, skin/cutaneous; CONJ, conjunctiva. *Bottom panel*: Comparison of nucleotide substitutions between the SCC cohorts. (**B**) Oncogenic pathway and hierarchical clustering analysis. The various SCC cohorts were analyzed for enrichment of mutations in genes involved in the oncogenic pathways listed on the *right*. The results are presented in *circular bar plots* that make up a constellation plot. In the constellation plot, the *outlined dark circle* in the *middle* represents the root of the hierarchical tree; the other *dark circles* represent cluster joints; the *lines* extending from each *dark circle* to one or more circular bar plots show the tumor types included in a cluster; the length of the *lines* between *dark circles* indicates the distance between clusters; and the tumor types are represented as end points. (**C**) Frequency of mutations in specific genes involved in each of the oncogenic pathways in the various SCC cohorts.

Investigative Ophthalmology & Visual Science

just reflect the link between CD8+ cell density and HPV infection.

Comparison of Genomic Characteristics Between ConjSCC and Other SCCs

To compare the genomic characteristics of conjSCC with those of other SCC subtypes, we retrieved whole exome sequencing data from SCCs from the bladder, uterine cervix, esophagus, head and neck, lungs, and skin available in the TCGA database (see Supplementary Table S1).

The mean (SD) TMB (number of mutations per MB, log 10) was significantly higher in our conjSCC cohort (3.01 [0.60]) than in every other SCC subtype except cutaneous SCC (Fig. 3A, Supplementary Table S9). When analyzed independently, the ETH samples had a significantly higher mean TMB (3.34 Mb) than any other SCC subtype, including cutaneous SCC (2.65 Mb), whereas the mean TMB in the MDA samples (2.73 Mb, SD = 0.60 Mb) was not significantly higher than that in the cutaneous SCC ($P = 1.00$) and lung SCC samples (2.33 Mb, $P = 0.327$; see Supplementary Table S9).

To compare the impact of HPV infection on the TMB between conjSCC and other tumors, we considered only head and neck SCC samples and grouped them according to HPV status (see Supplementary Table S9). Unlike what we found for conjSCCs, in head and neck SCCs, the mean (SD) TMB (number of mutations per MB, log 10) was significantly lower in HPV+ tumors than in HPV– tumors (1.88 [0.36] vs. 2.04 [0.33], $P < 0.001$). Interestingly, even HPV+ conjSCCs had a mean (SD) TMB higher than that of HPV– head and neck SCCs (2.74 [0.75] vs. 2.04 [0.33], $P = 0.005$).

Next, we compared the distribution of the types of nucleotide substitutions for each mutation in every SCC analyzed (see Fig. 3A). The frequencies of the types of nucleotide substitutions in conjSCC were significantly different from the pattern observed in SCCs from the bladder, uterine cervix, esophagus, head and neck, and lungs but highly similar to the pattern observed in cutaneous SCCs. On average, more than 70% of the nucleotide substitutions in conjSCC were C>T changes. Although C>T was also the most common substitution type in the other SCCs (except lung SCC), the frequency of C>T was significantly higher in conjSCC than in any other tumor except cutaneous SCC. The only significant difference between conjSCC and cutaneous SCC was the higher frequency of T>C substitutions in cutaneous SCC (7.2% vs. 4.5%, false discover rate [FDR] = 0.004; see Supplementary Table S8). This finding suggests that conjSCC and cutaneous SCC are similar not only in terms of high TMB, but also in terms of potential procarcinogenic molecular mechanisms.

Next, we compared the genomic profile of conjSCC to that of the other SCCs in terms of a curated list of cancer driver genes and their respective pathways.[48] For this, we used a pathway-centered analysis with the objective of unveiling the molecular mechanisms specific to conjSCC compared to SCCs of other organs.

After determining the frequency of mutations in the cancer driver genes according to their respective pathways, we performed hierarchical clustering analysis (Fig. 3B). The pathways with the highest numbers of mutant genes in SCCs included "Genome integrity" (an average of 74% of genes in the pathway were mutated), "Chromatin SWI/SNF complex" (54%), "Transcription factor" (50%), "Other signaling" (48%), and "Other" (47%). ConjSCC and cutaneous SCC clustered together and appeared to be highly distinct from the other SCC subtypes, with the most relevant differences noted in Wnt/B-catenin signaling, NOTCH signaling, splicing, and NFKB signaling.

The conjSCC and cutaneous SCC samples had the highest level of similarity. "Transcription Factor," "Genome integrity," "Other signaling," "Chromatin SWI/SNF complex," "Other," "RTK signaling," "Chromatin histone modifiers," and "Chromatin (other)" pathways were mutated in more than 50% of tumors in both cohorts. On the other hand, "Immune signaling" (56% vs. 28%, FDR = 0.002), "TOR signaling" (35% vs. 16%, FDR = 0.018), "Epigenetics DNA modifiers" (20% vs. 7%, FDR = 0.044), and "Metabolism" (9% vs. 1%, FDR = 0.046) pathways were mutated more frequently in conjSCC than in cutaneous SCC samples. The only significant difference between conjSCC and cutaneous SCC was a higher frequency of immune and TOR signaling in conjSCC (FDR = 0.002 and 0.018, respectively).

ConjSCCs were highly distinct from the other SCCs (excluding cutaneous SCC), with an overall higher number of patients with mutations in most of the pathways. Mutations in driver genes from the "Epigenetics DNA modifiers," "Immune signaling," and "TOR signaling" pathways had a higher frequency in conjSCC than in any other SCC subtype (Fig. 3C), in particular, the lungs, head and neck, and esophageal SCCs. Interestingly, genes from the "Transcription factor" pathway were the most frequently mutated in conjSCC (85% of samples) compared to other SCCs. Although this pathway is commonly affected by mutations in SCCs, the average number of affected patients is significantly lower considering all SCCs (50%) and each cohort individually (see Supplementary Table S9).

Discussion

Our histologic and genomic observations in this study suggest that UV exposure plays an important role in the etiopathogenesis of conjSCC and may play a more significant role in tumors arising in African patients than in tumors arising in North American patients. This hypothesis is supported by the presence of solar elastosis in 31% of conjSCCs, including 78% of those in the ETH cohort, but only 10% of the MDA cohort. We found that the SBS7b UV exposure–associated mutation signature was the most frequent mutation pattern in both cohorts with 37 patients (69%) and was associated with the highest number of mutations in both cohorts. This mutation signature was more prevalent in the ETH cohort than in the MDA cohort.

Another important finding in our study, and a finding that suggests potential new treatment options for conjSCC, is the high TMB of conjSCC. The TMB for conjSCC was similar to that of cutaneous SCC and higher than that of most other SCC subtypes. A high TMB for a given cancer has been correlated with expected response to immune checkpoint inhibitors.[49,50] One limitation of our study was that normal/germline DNA was available for only 13 MDA conjSCCs. Lack of availability of germline DNA for each of the tumor sample leaves open the possibility that some of the mutations seen in the conjSCC samples in our study could be background genetic alterations, not necessarily driver mutations. This possibility may be particularly relevant for the ETH cohort because germline data from African patients are not represented as highly as germline data from patients from other regions in most germline variant databases that

Investigative Ophthalmology & Visual Science

are used for filtering. However, the predominance of the UV signature in both cohorts indicates that the high TMB may be driven by UV-induced DNA damage rather than high burden of germline genetic alterations. So even if some germline variants are inflating the specific TMB values for our cohorts, it is likely that these tumors still have a high TMB due to UV damage.

We found evidence of high-risk HPV by in situ hybridization in 21% of conjSCCs in the ETH cohort and 28% of conjSCCs in the MDA cohort. A recent meta-analysis of 39 studies found a pooled HPV prevalence of 26% in patients with conjunctival intra-epithelial neoplasia and conjSCC, with HPV16, HPV18, and HPV33 the most frequently reported genotypes.[16] We further found that the genomic differences between HPV+ and HPV– conjSCCs from the MDA cohort resembled the differences observed in other tumors, such as oropharyngeal, head, and neck tumors. On the other hand, conjSCCs in the ETH cohort did not display the same differences between HPV+ and HPV– cases.

Additionally, our whole exome sequencing data suggest that the SBS2 and SBS13 mutation signatures were significantly more common among MDA HPV+ conjSCCs than among MDA HPV– conjSCCs and were absent in ETH conjSCCs ($P < 0.001$). These mutation signatures are thought to be associated with the activity of the AID/APOBEC family of cytidine deaminases. These mutation signatures have been previously described in HPV-associated tumors, and which were indeed enriched in HPV+ conjSCCs in the MDA cohort. However, none of the HPV+ tumors in the ETH cohort exhibited these signatures, which suggests that HPV+ conjSCCs in patients in Ethiopia and the United States are genetically distinct. It is also possible that environmental variables are responsible for these differences. Conjunctival solar elastosis was more common in the ETH cohort than in the MDA cohort, even among HPV+ cases. Furthermore, a high proportion of the conjSCCs in the ETH cohort had mutations in *TP53*. It is thought that HPV-derived E6 and E7 proteins obviate the requirement for *TP53* mutation to drive carcinogenesis, and thus *TP53* mutations are not usually found in HPV-driven tumors. Thus, it is possible that although HPV was present in some of the ETH tumors, it may not be the principal driver of conjSCC and may be rather a "passenger" in the process. For comparison, the MDA HPV+ tumors did not have *TP53* mutations at such a high frequency. Thus, it appears that HPV overall has a minor role in altering the genomic landscape of these tumors, compared to UV-induced DNA damage. This is an interesting biologically and potentially clinically relevant puzzle that deserves further investigation.

We found PD-L1 expression in 62% of conjSCCs and no significant difference in the rate of PD-L1 expression between the two cohorts (ETH = 54% and MDA = 69%). This value is similar to a 47% positivity rate that we reported in a previous study[26]; however, it is lower than the value in a more recent report from Boston.[51] We noted increased density of TILs in association with thicker tumors and increased density of CD3+, CD8+, and PD1+ TILs in association with PD-L1 positive tumors, a feature also reported in our previous study.[26] We also found increased density of CD8+ cells among HPV+ conjSCCs in the MDA cohort but not in the ETH cohort. The correlation among HPV status, PD-L1 expression, and TILs is yet to be established definitively in HPV-driven SCCs. Studies have revealed conflicting data, which may be attributed to relatively small size of cohorts, diversity of populations included in the studies, such as the broad variability of primary-tumor anatomic locations, and the associated risk factors. For instance, we did not identify a definitive correlation between HPV status and PD-L1 expression in the current or our previous studies of conjSCC, in line with findings from studies of SCCs arising from the anus,[52] oral cavity,[53] and oropharynx.[54] However, other studies have demonstrated correlations between p16 and PD-L1 expression[55] and between HPV status and PD-L1 expression in SCC of the oropharynx,[56] in which PD-L1 expression was higher among HPV+ cases and higher PD-L1 expression also correlated with longer disease-specific and overall survival. The same study also demonstrated better prognosis among patients with CD8+ TILs, particularly when associated with HPV+ status[56] or p16 expression.[57] In oropharyngeal SCC, HPV positivity or p16 expression has been associated with higher density of TILS,[58] including CD8+ TILs, which also appeared to correlate with longer OS.[57,59,60]

In conclusion, our findings demonstrate that in African patients, UV exposure has a major role in the development of the mutational background of conjSCC, whereas in North American patients, both UV exposure and HPV infection are linked to distinct mutation profiles. Our data from whole exome sequencing combined with our histologic observations suggest that UV exposure may be more important than HPV in the development of conjSCC. Our study had several limitations, including its retrospective nature, which limited the tissue for our study to archived material rather than fresh frozen tumor samples, which limited availability of germline DNA for the majority of our tumors. In addition, the majority of the ETH conjSCCs were large compared to an archetypal MDA conjSCC. In order to have adequate tumor volume, we had to choose relatively larger/ advanced conjSCC samples for the MDA cohort, which may partly explain the presence of PNI and LVI in MDA samples, compared to the ETH cohort. A major conflict and war in Ethiopia prevented our collaborating partners from accessing the clinical data for the ETH cohort; thus, we were not able to do reliable clinical correlation for some of our genomic and pathologic observations. Nevertheless, to our knowledge, this is one of the few comprehensive genomic and histopathologic studies to compare findings between an African cohort and a North American cohort of patients with conjSCC. It is also, to our knowledge, the first study to focus on UV exposure and solar elastosis as important contributors to the prevalence and severity of conjSCC in sub-Saharan Africa. It is also, to our knowledge, the first study to report PD-L1 expression in more than half of conjSCCs in a sub-Saharan African cohort and report a high TMB for conjSCC, opening the possibility that immune checkpoint inhibitors could be considered for treatment of locally advanced and/or metastatic conjSCC.

Acknowledgments

The authors thank Stephanie Deming, Research Medical Library, MD Anderson Cancer Center, for editing the manuscript.

Supported by the NIH/NCI under award number P30CA016672.

Disclosure: **F.O. Gleber-Netto**, None; **P. Nagarajan**, None; **O. Sagiv**, None; **C.R. Pickering**, None; **N. Gross**, None; **J. Ning**; None; **M.M. Yeshi**, None; **Y. Mitku**, None; **M.T. Tetzlaff**, None; **B. Esmaeli**, None

References

1. Karcioglu ZA, Wagoner MD. Demographics, etiology, and behavior of conjunctival squamous cell carcinoma in the 21st century. *Ophthalmology*. 2009;116(11):2045–2046.
2. Gichuhi S, Sagoo MS, Weiss HA, Burton MJ. Epidemiology of ocular surface squamous neoplasia in Africa. *Trop Med Int Health*. 2013;18(12):1424–1443.
3. Shields CL, Ramasubramanian A, Mellen PL, Shields JA. Conjunctival squamous cell carcinoma arising in immunosuppressed patients (organ transplant, human immunodeficiency virus infection). *Ophthalmology*. 2011;118(11):2133–2137.e1.
4. El-Hadad C, Rubin ML, Nagarajan P, et al. Prognostic factors for orbital exenteration, local recurrence, metastasis, and death from disease in conjunctival squamous cell carcinoma. *Ophthalmic Plast Reconstr Surg*. 2021;37(3):262–268.
5. Newton R, Ziegler J, Ateenyi-Agaba C, et al. The epidemiology of conjunctival squamous cell carcinoma in Uganda. *Br J Cancer*. 2002;87(3):301–308.
6. Kaimbo Wa Kaimbo D, Parys-Van Ginderdeuren R, Missotten L. Conjunctival squamous cell carcinoma and intraepithelial neoplasia in AIDS patients in Congo Kinshasa. *Bull Soc Belge Ophtalmol*. 1998;268:135–141.
7. Chisi SK, Kollmann MK, Karimurio J. Conjunctival squamous cell carcinoma in patients with human immunodeficiency virus infection seen at two hospitals in Kenya. *East Afr Med J*. 2006;83(5):267–270.
8. Poole TR. Conjunctival squamous cell carcinoma in Tanzania. *Br J Ophthalmol*. 1999;83(2):177–179.
9. Ateenyi-Agaba C. Conjunctival squamous-cell carcinoma associated with HIV infection in Kampala, Uganda. *Lancet (London, England)*. 1995;345(8951):695–696.
10. Waddell KM, Lewallen S, Lucas SB, Atenyi-Agaba C, Herrington CS, Liomba G. Carcinoma of the conjunctiva and HIV infection in Uganda and Malawi. *Br J Ophthalmol*. 1996;80(6):503–508.
11. Gichuhi S, Macharia E, Kabiru J, et al. Clinical presentation of ocular surface squamous neoplasia in Kenya. *JAMA Ophthalmol*. 2015;133(11):1305–1313.
12. Peters RPH, Kestelyn PG, Zierhut M, Kempen JH. The changing global epidemic of HIV and ocular disease. *Ocul Immunol Inflamm*. 2020;28(7):1007–1014.
13. Gichuhi S, Kabiru J, M'Bongo Zindamoyen A, et al. Delay along the care-seeking journey of patients with ocular surface squamous neoplasia in Kenya. *BMC Health Serv Res*. 2017;17(1):485.
14. Kiire CA, Dhillon B. The aetiology and associations of conjunctival intraepithelial neoplasia. *Br J Ophthalmol*. 2006;90(1):109–113.
15. Yu JJ, Fu P, Pink JJ, et al. HPV infection and EGFR activation/alteration in HIV-infected East African patients with conjunctival carcinoma. *PLoS One*. 2010;5(5):e10477.
16. Ramberg I, Møller-Hansen M, Toft PB, Funding M, Heegaard S. Human papillomavirus infection plays a role in conjunctival squamous cell carcinoma: a systematic review and meta-analysis of observational studies. *Acta Ophthalmol*. 2021;99(5):478–488.
17. Jayaraj P, Sen S, Saxena K, et al. Immunohistochemical and mutational status of telomerase reverse transcriptase in conjunctival squamous cell carcinoma. *Indian J Ophthalmol*. 2022;70(3):971–975.
18. Tagami M, Kakehashi A, Sakai A, et al. Expression of thrombospondin-1 in conjunctival squamous cell carcinoma is correlated to the Ki67 index and associated with progression-free survival. *Graefes Arch Clin Exp Ophthalmol*. 2021;259(10):3127–3136.
19. Tornesello ML, Waddell KM, Duraturo ML, et al. TP53 codon 72 polymorphism and risk of conjunctival squamous cell carcinoma in Uganda. *Cancer Detect Prev*. 2005;29(6):501–508.
20. Karcioglu ZA, Toth J. Relation between p53 overexpression and clinical behavior of ocular/orbital invasion of conjunctival squamous cell carcinoma. *Ophthalmic Plast Reconstr Surg*. 2000;16(6):443–449.
21. Mahale A, Alkatan H, Alwadani S, et al. Altered gene expression in conjunctival squamous cell carcinoma. *Mod Pathol*. 2016;29(5):452–460.
22. Gross ND, Miller DM, Khushalani NI, et al. Neoadjuvant cemiplimab for stage II to IV cutaneous squamous-cell carcinoma. *N Engl J Med*. 2022;387(17):1557–1568.
23. Ferrarotto R, Amit M, Nagarajan P, et al. Pilot phase II trial of neoadjuvant immunotherapy in locoregionally advanced, resectable cutaneous squamous cell carcinoma of the head and neck. *Clin Cancer Res*. 2021;27(16):4557–4565.
24. Migden MR, Rischin D, Schmults CD, et al. PD-1 blockade with cemiplimab in advanced cutaneous squamous-cell carcinoma. *N Engl J Med*. 2018;379(4):341–351.
25. Goldfarb JA, Ferrarotto R, Gross N, et al. Immune checkpoint inhibitors for treatment of periorbital squamous cell carcinoma. *Br J Ophthalmol*. 2023;107(3):320–323.
26. Nagarajan P, El-Hadad C, Gruschkus SK, et al. PD-L1/PD1 expression, composition of tumor-associated immune infiltrate, and HPV status in conjunctival squamous cell carcinoma. *Invest Ophthalmol Vis Sci*. 2019;60(6):2388–2398.
27. Li H, Durbin R. Fast and accurate short read alignment with Burrows-Wheeler transform. *Bioinformatics*. 2009;25(14):1754–1760.
28. DePristo MA, Banks E, Poplin R, et al. A framework for variation discovery and genotyping using next-generation DNA sequencing data. *Nat Genet*. 2011;43(5):491–498.
29. Cibulskis K, Lawrence MS, Carter SL, et al. Sensitive detection of somatic point mutations in impure and heterogeneous cancer samples. *Nat Biotechnol*. 2013;31(3):213–219.
30. Karczewski KJ, Weisburd B, Thomas B, et al. The ExAC browser: displaying reference data information from over 60 000 exomes. *Nucleic Acids Res*. 2017;45(D1):D840–D845.
31. Genomes Project C, Auton A, Brooks LD, et al. A global reference for human genetic variation. *Nature*. 2015;526(7571):68–74.
32. Chen S, Francioli LC, Goodrich JK, et al. A genome-wide mutational constraint map quantified from variation in 76,156 human genomes. *bioRxiv* 2022:2022.03.20.485034.
33. Robinson JT, Thorvaldsdottir H, Wenger AM, Zehir A, Mesirov JP. Variant review with the integrative genomics viewer. *Cancer Res*. 2017;77(21):e31–e34.
34. Wang N, Lysenkov V, Orte K, et al. Tool evaluation for the detection of variably sized indels from next generation whole genome and targeted sequencing data. *PLoS Comput Biol*. 2022;18(2):e1009269.
35. Wong SQ, Li J, Salemi R, et al. Targeted-capture massively-parallel sequencing enables robust detection of clinically informative mutations from formalin-fixed tumours. *Sci Rep*. 2013;3:3494.
36. Mayakonda A, Lin DC, Assenov Y, Plass C, Koeffler HP. Maftools: efficient and comprehensive analysis of somatic variants in cancer. *Genome Res*. 2018;28(11):1747–1756.
37. Roberts SA, Lawrence MS, Klimczak LJ, et al. An APOBEC cytidine deaminase mutagenesis pattern is widespread in human cancers. *Nat Genet*. 2013;45(9):970–976.
38. Bergstrom EN, Huang MN, Mahto U, et al. SigProfilerMatrixGenerator: a tool for visualizing and exploring patterns of small mutational events. *BMC Genomics*. 2019;20(1):685.
39. Islam SMA, Díaz-Gay M, Wu Y, et al. Uncovering novel mutational signatures by de novo extraction with SigProfilerExtractor. *Cell Genom*. 2022;2(11):None.

Investigative Ophthalmology & Visual Science

40. Bergstrom EN, Luebeck J, Petljak M, et al. Mapping clustered mutations in cancer reveals APOBEC3 mutagenesis of ecDNA. *Nature*. 2022;602(7897):510–517.
41. Campbell JD, Yau C, Bowlby R, et al. Genomic, pathway network, and immunologic features distinguishing squamous carcinomas. *Cell Rep*. 2018;23(1):194–212.e6.
42. Ellrott K, Bailey MH, Saksena G, et al. Scalable open science approach for mutation calling of tumor exomes using multiple genomic pipelines. *Cell Syst*. 2018;6(3):271–281.e7.
43. 2016 Broad Institute TCGA Genome Data Analysis Center (2016): Mutation Analysis (MutSig 2CV v3.1). Broad Institute of MIT and Harvard.
44. Chang D, Shain AH. The landscape of driver mutations in cutaneous squamous cell carcinoma. *NPJ Genom Med*. 2021;6(1):61.
45. Bailey MH, Tokheim C, Porta-Pardo E, et al. Comprehensive characterization of cancer driver genes and mutations. *Cell*. 2018;173(2):371–385.e18.
46. Martinez-Jimenez F, Muinos F, Sentis I, et al. A compendium of mutational cancer driver genes. *Nat Rev Cancer*. 2020;20(10):555–572.
47. Gillison ML, Akagi K, Xiao W, et al. Human papillomavirus and the landscape of secondary genetic alterations in oral cancers. *Genome Res*. 2019;29(1):1–17.
48. Bailey MH, Tokheim C, Porta-Pardo E, et al. Comprehensive characterization of cancer driver genes and mutations. *Cell*. 2018;173(2):371–385.e18.
49. Wu Y, Xu J, Du C, et al. The Predictive value of tumor mutation burden on efficacy of immune checkpoint inhibitors in cancers: a systematic review and meta-analysis. *Front Oncol*. 2019;9:1161.
50. Ning B, Liu Y, Wang M, Li Y, Xu T, Wei Y. The predictive value of tumor mutation burden on clinical efficacy of immune checkpoint inhibitors in melanoma: a systematic review and meta-analysis. *Front Pharmacol*. 2022;13:748674.
51. Wolkow N, Jakobiec FA, Afrogheh AH, Eagle RC, Jr., Pai SI, Faquin WC. Programmed cell death 1 ligand 1 and programmed cell death 1 ligand 2 are expressed in conjunctival invasive squamous cell carcinoma: therapeutic implications. *Am J Ophthalmol*. 2019;200:226–241.
52. Wessely A, Heppt MV, Kammerbauer C, et al. Evaluation of PD-L1 expression and HPV genotyping in anal squamous cell carcinoma. *Cancers (Basel)*. 2020;12(9):2516.
53. Kitichotkul K, Lertprasertsuke N, Kintarak S, Pongsiriwet S, Powcharoen W, Iamaroon A. Expression of PD-L1 is HPV/P16-independent in oral squamous cell carcinoma. *Heliyon*. 2022;8(10):e10667.
54. Kim HS, Lee JY, Lim SH, et al. Association between PD-L1 and HPV status and the prognostic value of PD-L1 in oropharyngeal squamous cell carcinoma. *Cancer Res Treat*. 2016;48(2):527–536.
55. Kareer R, Ahuja S, Chaudhary N, Arora R. Association of PD-L1 and p16 expression with clinicopathological parameters in oral cavity and oropharyngeal squamous cell carcinoma. *Pathol Res Pract*. 2023;241:154266.
56. Zhu Y, Zhu X, Diao W, Liang Z, Gao Z, Chen X. Correlation of immune makers with HPV 16 infections and the prognosis in oropharyngeal squamous cell carcinoma. *Clin Oral Investig*. 2023;27(4):1423–1433.
57. Atipas K, Laokulrath N, Petsuksiri J, Ratanaprasert N, Pongsapich W. CD8+ T cells and PD-L1 expression as prognostic indicators in a low prevalence of HPV-associated oropharyngeal squamous cell carcinoma. *Curr Oncol*. 2023;30(2):1450–1460.
58. Tosi A, Parisatto B, Menegaldo A, et al. The immune microenvironment of HPV-positive and HPV-negative oropharyngeal squamous cell carcinoma: a multiparametric quantitative and spatial analysis unveils a rationale to target treatment-naive tumors with immune checkpoint inhibitors. *J Exp Clin Cancer Res*. 2022;41(1):279.
59. Solomon B, Young RJ, Bressel M, et al. Prognostic significance of PD-L1(+) and CD8(+) immune cells in HPV(+) oropharyngeal squamous cell carcinoma. *Cancer Immunol Res*. 2018;6(3):295–304.
60. Masterson L, Lechner M, Loewenbein S, et al. CD8(+) T cell response to human papillomavirus 16 E7 is able to predict survival outcome in oropharyngeal cancer. *Eur J Cancer*. 2016;67:141–151.